Divalent Cation Selectivity in a Cyclic Nucleotide-Gated Ion Channel†

Chul-Seung Park and Roderick MacKinnon*

Department of Neurobiology, 220 Longwood Avenue, Harvard Medical School, Boston, Massachusetts 02115

Received June 13, 1995; Revised Manuscript Received August 14, 1995®

ABSTRACT: Divalent metal cation selectivity was studied in guanosine 3′,5′-cyclic monophosphate-gated ion channels. Channels from bovine retina were expressed in *Xenopus laevis* oocytes, and currents were measured using tight-seal patch recording methods. The ability of divalent cations to block Na^+ currents was used to determine the occupancy of divalent cations in the ion conduction pore. At positive membrane voltages, where extracellular divalent cations are near equilibrium with their binding site, the occupancy reflects the affinity of the blocking ion. The selectivity sequence based on relative affinity was $Ca^{2+} > Mg^{2+} = Sr^{2+} = Ba^{2+}$. In addition to its higher affinity, Ca^{2+} was more permeant and blocked with a weaker voltage dependence. Ca^{2+} was the only ion that blocked with a high Hill coefficient ($n = 2.7$), suggesting the presence of multiple binding sites. When Glu 363, located in the pore-forming region, was mutated to Asp, the affinity of all four ions increased and the selectivity sequence became $Ca^{2+} > Sr^{2+} > Ba^{2+} > Mg^{2+}$. These results show that the channel is highly selective for Ca^{2+} and that Glu 363 mediates divalent cation selectivity of the channel.

Cyclic nucleotide-gated (CNG)[1] channels are cation channels that open in response to the direct binding of intracellular cGMP or cAMP [for review, see Yau and Chen (1995)]. When these channels are open, they conduct monovalent and divalent cations (Stern et al., 1987; Menini et al., 1988; Colamartino et al., 1991; Zimmerman & Baylor, 1992). The very different rates at which these cations conduct have physiological relevance. In physiological solutions, the slowly permeating Ca^{2+} and Mg^{2+} ions reduce the through put of the otherwise rapidly permeating Na^+ ions. In retinal CNG channels, this blockade of Na^+ current by extracellular Mg^{2+} and Ca^{2+} allows a low noise membrane potential necessary for the sensitive detection of dim light (Yau & Baylor, 1989). At the same time, Ca^{2+} entering the cell influences light adaptation, which is required for a broad dynamic range of light sensitivity (Kaupp & Koch, 1991; Koutalos & Yau, 1993).

The proposed membrane topology of a CNG channel α subunit is shown in Figure 1A. Although more than one subunit type may be important in nature, the α subunit alone is sufficient to produce functional channels through the formation of homomultimers (probably tetramers) when expressed in *Xenopus* oocytes (Kaupp et al., 1989; Chen et al., 1993). Past work has identified a short segment of amino acids called the P-region (Goulding et al., 1993; Root & MacKinnon, 1993). This region, by reaching into the central pore, determines many of the ion conduction properties of the channel (MacKinnon, 1995). One specific residue, Glu 363 in Figure 1A, plays a particularly critical role. It is responsible for the manner in which Na^+ conductance saturates, and it influences the affinity of divalent cation blockade (Root & MacKinnon, 1993; Eismann et al., 1994; M. J. Root and R. MacKinnon, personal communication).

The focus of this study is to assess the role of Glu 363 in determining the selectivity among divalent cations. We estimated the affinity of a series of alkaline earth cations by making use of their ability to block Na^+ permeation through the channel. The binding site was highly selective for Ca^{2+} which is also the most permeant among the ions tested. A chemically conservative mutation of this residue (Glu → Asp) increased the affinity for all divalent cations but to different extents. Consequently, the mutation brings about a shift in the pattern of selectivity toward larger ions. These results argue that Glu 363 participates directly in the coordination of divalent cation(s) in the pore.

MATERIALS AND METHODS

Materials. Female *Xenopus laevis* were purchased from Xenopus One (Ann Arbor, MI). Restriction enzymes and T7 RNA polymerase were purchased from New England Biolabs (Beverly, MA) and Promega (Madison, WI), respectively. Collagenase was from Worthington Biochemical (Freehold, NJ). Cyclic GMP and other chemicals were purchased from either Sigma (St. Louis, MO) or Fisher (Pittsburgh, PA). The cDNA of the cGMP-gated channel α subunit from bovine retina (Goulding et al., 1992) was subcloned into the pGH vector containing 5′- and 3′-untranslated regions of the *Xenopus* β-globin gene for high-level expression (Liman et al., 1992). The preparation of the E363D mutation was previously described (Root & MacKinnon, 1993).

Expression of CNG Channels. The wild type and mutant (E363D) channels were expressed in *Xenopus* oocytes for electrophysiological studies as described previously (Root & MacKinnon, 1993). cRNA's for the wild type and mutant CNG channels were synthesized *in vitro* from an *Nhe*I-linearized plasmid using T7 RNA polymerase. Oocytes were injected with approximately 50 ng and 0.1 ng of RNA for macroscopic (many channels per patch) and single channel experiments, respectively. Injected oocytes were incubated

† This work was supported by NIH Grant GM47400 to R.M.

* Please send editorial comments to Dr. Roderick MacKinnon, Department of Neurobiology, 220 Longwood Avenue, Boston, MA 02115. Telephone: 617-432-1758. Fax: 617-734-7557.

® Abstract published in *Advance ACS Abstracts,* October 1, 1995.

[1] Abbreviations: CNG channel, cyclic nucleotide-gated channel; cGMP or cG, guanosine 3′,5′-cyclic monophosphate; Glu, glutamate; Asp, aspartate; P-region, pore-forming region.

0006-2960/95/0434-13328$09.00/0

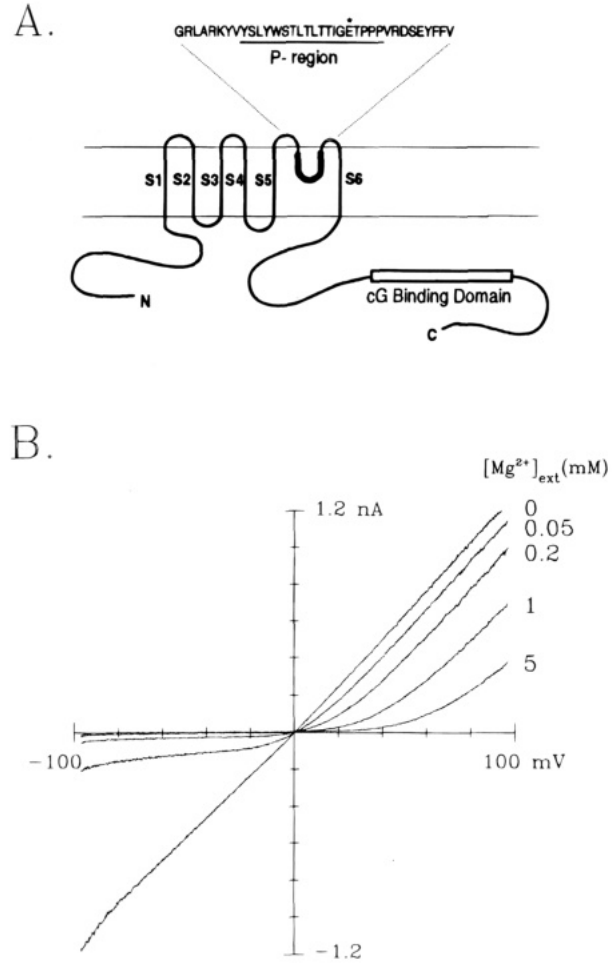

FIGURE 1: Membrane topology and external divalent blockade of CNG channels. (A) The proposed membrane topology and amino acid sequence of the S5−S6 linker region in a single α subunit of the bovine retinal CNG channel are shown. Glu 363 in the P-region is marked with an asterisk. (B) Na^+ currents through many channels in an outside-out membrane patch are blocked as Mg^{2+} concentration is raised in the extracellular (bath) solution. The pipette contained 500 μM cGMP to activate the channels. Membrane voltage was held at 0 mV and ramped from −100 to 100 mV over 820 ms. The membrane voltage refers to ground on the extracellular side of the patch. The records shown are averages of five individual ramps.

at 18 °C for 1−5 days in ND96 solution containing (in millimolar) 5 HEPES, 96 NaCl, 2 KCl, 1.8 $CaCl_2$, and 1 $MgCl_2$ and 50 μg/mL gentamicin, pH 7.6 (NaOH).

Electrophysiological Recording. Ionic currents carried by CNG channels were recorded from patches of oocyte membrane in the outside-out configuration using an Axopatch 200A amplifier (Axon Instruments, Foster City, CA). Signals were filtered at 1 or 2 kHz using a four-pole low-pass Bessel filter and digitized at the rate of 10 points/ms using a Microstar 3200e analog to digital converter (Microstar, Bellevue, WA) and personal computer (Gateway2000, North Sioux City, SD). Data were stored on computer disk for subsequent analysis. For macroscopic current recordings, the membrane was held at 0 mV and ramped from −100 to 100 mV over 820 ms. In order ensure that steady state blockade was achieved throughout the ramp, blockade was determined using an independent protocol of voltage steps lasting 100 ms. These control experiments gave the same result and therefore validated the use of ramps to accurately measure blockade (voltage steps were used in the case of Ca^{2+} blocking the E363D mutant channel where the high affinity would most likely result in an artifact using the ramp protocol). Membrane patches with currents between 0.5 and 2 nA (at 100 mV) were used for experiments. Single channels were recorded by holding the membrane voltage at −80 mV. Unless otherwise specified, both intracellular (pipette) and extracellular (bath) solutions contained the following components (in mM): 130 NaOH, 3 HEPES (free acid), 0.5 Na_2-EDTA (for Mg^{2+}-, Sr^{2+}-, and Ba^{2+}-containing solutions), or 5 Na_2-EGTA (for Ca^{2+}-containing solutions); both solutions were titrated to pH 7.6 using concentrated HCl. cGMP (500 μM) was added into the intracellular solution before the final pH adjustment. For external divalent cation solutions, the Cl^- salt of each divalent cation was added to give the desired free concentration calculated using the following stability constants (log *K*): Mg-EDTA, 8.83; Ca-EGTA, 10.86; Sr-EDTA, 8.68; and Ba-EDTA, 7.8 (Martell & Smith, 1974). The calculation included an adjustment for pH (Wolf, 1973). Blockade was measured by perfusing the extracellular face of the membrane patch with solutions containing different concentrations of divalent cations. Rapid and complete solution changes could be obtained by moving the patch sequentially across a linear array of microcapillary tubes, each containing a different concentration of blocking ion (1 μL, 64 mm length; Drummond). After control currents (in the absence of divalent cations) and blocked currents (in the presence of divalent cations) were recorded, each patch was perfused with solution containing 20 mM Mg^{2+}. Only patches with minimal residual current (less then 10 pA at 30 mV) were used for analysis.

RESULTS

Effect of Channel Gating on Extracellular Divalent Cation Blockade. The effect of extracellular Mg^{2+} on Na^+ currents through CNG channels is shown in Figure 1B. Inhibition (blockade) of the channel current is more extreme at negative membrane voltages, as if Mg^{2+} is driven into the pore. When Mg^{2+} concentration is increased, blockade becomes greater at all voltages. From measurements such as these, blocking titration curves can be generated. Since the goal of this work is to infer the affinity of an ion binding site on the basis of functional blockade, we first determined whether channel gating can affect the measurements.

In Figure 2, we asked whether the channel must be open to allow a divalent cation to reach its site from the extracellular solution. The channel open probability can be controlled by setting the cGMP concentration on the intracellular side of the patch. At 50 μM cGMP, the open probability is about 0.2, and at 500 μM, it is near 0.8 (Root & MacKinnon, 1993). Figure 2A shows titration curves for extracellular Sr^{2+} blocking the channel in the presence of 50 and 500 μM intracellular cGMP. The difference in open probability changes the half-blocking concentration, $K_{1/2}$, of Sr^{2+} from 5.9 μM (in 50 μM cGMP) to 14.1 μM (in 500 μM cGMP). The effect of gating on the Sr^{2+} affinity is modest and in the opposite direction expected if Sr^{2+} could only block the open channel. The result implies that the Sr^{2+} blocking site is accessible to extracellular ions, independent of the gating state of the channel. A similar result was observed for extracellular Mg^{2+} in a previous study (Karpen et al., 1993). At the level of single channels, Sr^{2+} reduces the open channel current amplitude in a manner

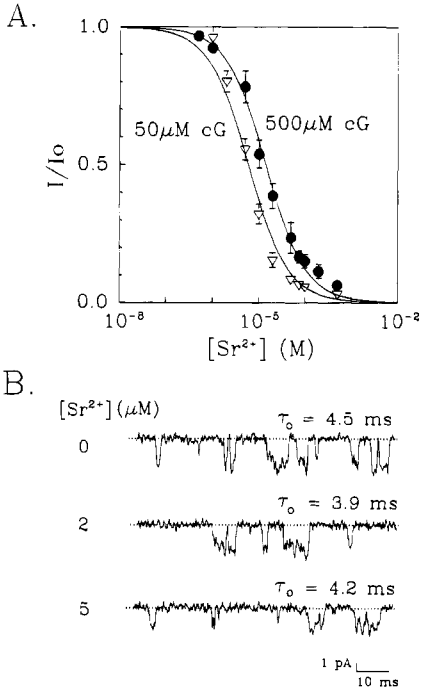

FIGURE 2: Effects of channel gating on extracellular Sr^{2+} blockade. (A) The fraction of unblocked current (I/I_o) at −80 mV is plotted as a function of the extracellular Sr^{2+} concentration in the presence of 50 and 500 μM intracellular cGMP. Channel open probability is about 0.2 and 0.8 in the presence of 50 and 500 μM cGMP, respectively. Each point is the mean ± the standard error of the mean of five separate experiments. Curves corresponding to the equation $I/I_o = (1 + [Sr^{2+}]^n/K_{1/2}^n)^{-1}$ give $K_{1/2}$ values of 5.9 μM, n = 1.1 (50 μM cGMP), and 14.1 μM, n = 1.0 (500 μM cGMP). (B) The effect of extracellular Sr^{2+} on a single channel is shown. Individual openings are downward from the closed channel level (dashed line). The membrane voltage was −80 mV, and τ_o, the mean open dwell time, was calculated from records that were idealized on the basis of crossing a 40−60% current level threshold.

characteristic of a filtered blocking process (Figure 2B). The mean duration of channel openings is unaffected by addition of Sr^{2+} to the extracellular solution. A blocker of only the open channel would lengthen these intervals. It appears that the divalent cation binding site is not hidden when the channel gate is closed.

Divalent Cations Are Permeant Blockers of the Channel. Figure 3 shows the complicated voltage-dependent behavior of divalent cation blockade. As the membrane voltage is made progressively more negative, the degree of blockade first increases and then decreases. This biphasic response can be understood in terms of divalent cation permeation (Zimmerman & Baylor, 1992). While more negative membrane voltages favor entry of a blocking cation from the extracellular solution, they also drive the blocker all the way through to the intracellular side. At very negative voltages, permeation of the blocker begins to dominate. Ca^{2+} is the most permeant in this regard and Mg^{2+} the least.

Permeation of a blocking cation creates a problem if we wish to determine the affinity of a blocker for its binding site. In general, the degree to which a permeant blocker reduces current carried by a second ion (Na^+ in this case) is a measure of the steady state (not equilibrium) occupancy of the site by the blocking ion. Therefore, we wished to identify conditions where the blocking ion is close to being at equilibrium with its site. We began by measuring blockade under true equilibrium conditions (Figure 4).

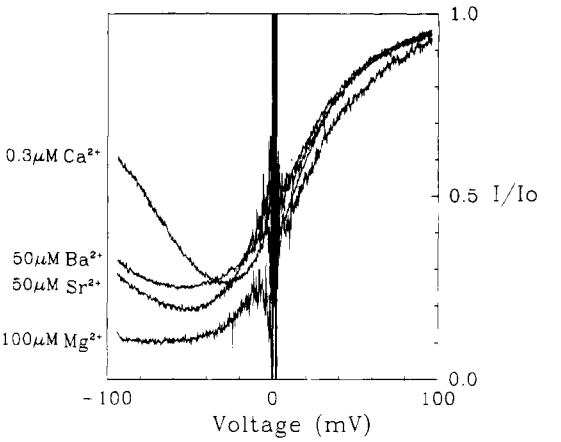

FIGURE 3: Ca^{2+} is the most permeant of the divalent cations tested. The fraction of unblocked current (I/I_o) is plotted against membrane voltage for extracellular Mg^{2+}, Ca^{2+}, Sr^{2+}, and Ba^{2+} present at the indicated concentrations. The recordings for each ion were made in separate outside-out patches while membrane voltage was ramped from −100 to 100 mV over 820 ms. The ratio (I/I_o) was calculated using traces consisting of an average of five consecutive ramps in the absence and presence of blocking ion.

Current−voltage curves were measured with identical Na^+ and Mg^{2+} concentrations on both sides of the membrane (Figure 4A, 100/100 trace). The blockade observed at 0 mV (from the slope of the current−voltage curve) is thus blockade occurring at equilibrium. Because the measurement was carried out using an outside-out patch, the control record (zero external Mg^{2+}) was not at equilibrium. However, we found in separate experiments that the concentrations of internal Mg^{2+} used in this experiment did not block the channel at 0 mV (data not shown). A titration curve for block at equilibrium (Figure 4B) shows that Mg^{2+} binds in the pore with a $K_{i,eq}$ of about 60 μM. Figure 4C compares the equilibrium value with half-blocking concentrations obtained at several membrane voltages. At membrane voltages more positive than −40 mV, the $K_{1/2}$ values are an exponential function of the membrane voltage, as one often observes for a nonpermeant blocker binding to a site in the transmembrane electric field (Woodhull, 1973). Thus, we can make a reasonable estimate of a blocking ion's affinity for the pore under conditions where the blocker associates and dissociates with its site from the same side of the membrane. On the basis of this observation, the $K_{1/2}$ measured at positive voltages reflects the affinity.

Selectivity among Divalent Cations Is Conferred by Glu 363. Figure 5A shows blocking curves for external Mg^{2+}, Ca^{2+}, Sr^{2+}, and Ba^{2+} measured at 30 mV. Ca^{2+} is outstanding in two respects. It blocks the channel with a much higher affinity than the other ions, and its blocking curve is very steep, as was described previously (Eismann et al., 1994). While ions other than Ca^{2+} block with similar affinities and Hill coefficients (0.9−1.1), Ca^{2+} blocks with a Hill coefficient of 2.7.

A chemically conservative mutation at position 363 (Glu → Asp) has a dramatic effect on the profile of blockade by external divalent cations (Figure 5B). This mutation decreases $K_{1/2}$ for all ions but not in a uniform manner. The largest change in affinity was observed for Sr^{2+} where $K_{1/2}$ decreased from 91 to 0.57 μM. We further studied this large change in affinity at the level of single channels (Figure 6). For the wild type channel, 10 μM Sr^{2+}, a roughly half-

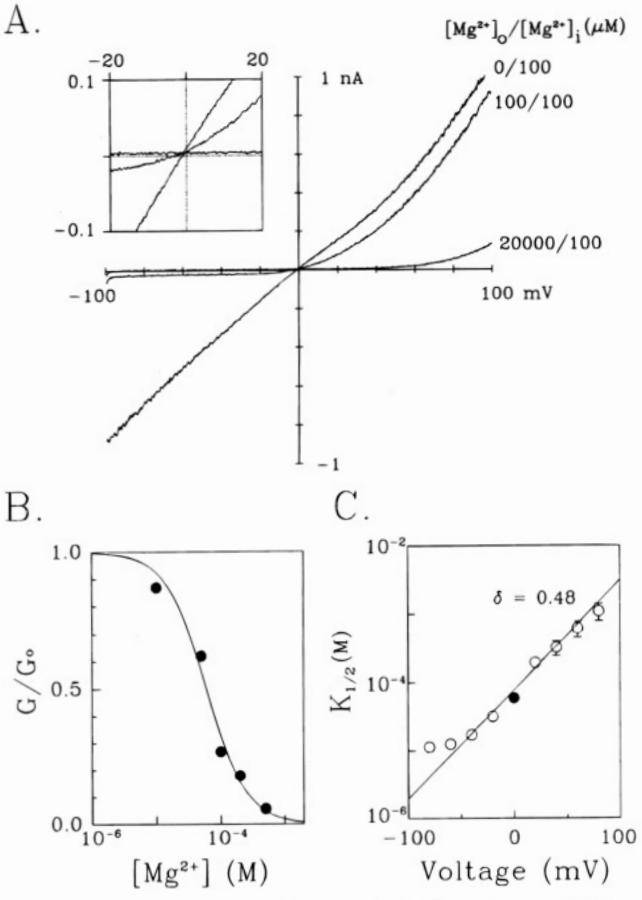

FIGURE 4: Measurement of Mg^{2+} blockade under equilibrium conditions. (A) Na^+ currents through an outside-out patch containing many channels were recorded in the presence of the indicated Mg^{2+} concentrations on each side of the membrane. The solutions are otherwise as described in the Materials and Methods. Each trace shown is an average of five consecutive records. The inset shows an expanded scale near the origin of the graph. (B) The conductance G is the slope of the current−voltage curve at 0 mV measured with equal concentrations of Mg^{2+} on both sides of the membrane. G_o is the slope measured in the absence of extracellular Mg^{2+}. The ratio G/G_o is plotted as a function of Mg^{2+} concentration and represents the blockade by Mg^{2+} at equilibrium. Data points were fit to a 1:1 binding function (see legend of Figure 2) with $K_{i,eq}$ = 60 μM, n = 1.0 (solid curve). (C) $K_{1/2}$ for Mg^{2+} blockade is plotted as a function of membrane voltage (empty circles). $K_{i,eq}$, 60 μM, determined in part B is shown as a filled circle. The straight line corresponds to the equation $K_{1/2} = K_{1/2}(0\text{ mV})\exp(z\delta FV/RT)$, where V is membrane voltage, $K_{1/2}(0\text{ mV})$ = 69 μM, the blocker valence z = 2, and the fractional distance across the membrane potential drop δ = 0.46.

blocking concentration at −80 mV, produces a reduction in the single channel amplitude (Figure 6A). This result is expected if the blocker associates and dissociates with kinetics that are too rapid to be resolved by the recording system; discrete blocking events become filtered. Sr^{2+} has a very different effect on the mutant single channel that has a larger single channel conductance (Figure 6B). It induces long nonconducting intervals that undoubtedly correspond to the dwell time of the blocking ion. Therefore, the increased affinity exhibited by the mutant channel is due at least in part to a smaller blocker dissociation rate constant.

The graphs in Figure 7 show the voltage dependence of $K_{1/2}$ for all four ions in both the wild type and the mutant channel. As we observed in Figure 3, at positive voltages, $K_{1/2}$ depends exponentially on membrane voltage; the dependence is similar for Mg^{2+}, Sr^{2+}, and Ba^{2+} (δ = 0.40−0.46) but is weaker for Ca^{2+} (δ = 0.22). It is striking to see that the mutation E363D has a proportional effect on affinity at all voltages (Figure 7). That is, there is a voltage-independent energy offset. The value of the offset is different

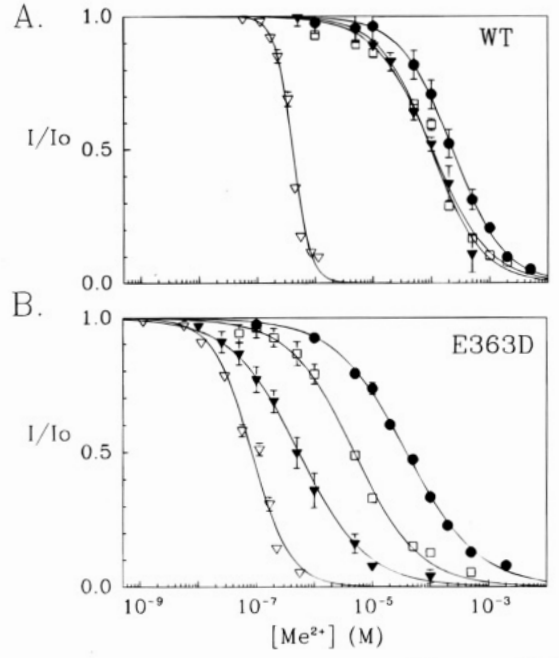

FIGURE 5: Divalent cation selectivity of the wild type and E363D mutant channels. (A) Fraction of unblocked current (I/I_o) at 30 mV in the wild type channel is plotted as a function of divalent cation concentration. The data are fit to the equation $I/I_o = (1 + [Me^{2+}]^n/K_{1/2}^n)^{-1}$ with blocking constant $K_{1/2}$ (in micromolar) and Hill coefficient n: Mg^{2+} (filled circles), $K_{1/2}$ = 260 ± 40, n = 1.1 ± 0.1; Ca^{2+} (empty triangles), $K_{1/2}$ = 0.38 ± 0.03, n = 2.7 ± 0.2; Sr^{2+} (filled triangles), $K_{1/2}$ = 91 ± 7, n = 1.0 ± 0.2; Ba^{2+} (empty squares), $K_{1/2}$ = 104 ± 9, n = 1.1 ± 0.1. (B) The corresponding data for the mutant E363D channel are shown with the following values for each ion: Mg^{2+} (filled circles), $K_{1/2}$ = 39 ± 4, n = 0.9 ± 0.1; Ca^{2+} (empty triangles), $K_{1/2}$ = 0.053 ± 0.011, n = 1.3 ± 0.3; Sr^{2+} (filled triangles), $K_{1/2}$ = 0.57 ± 0.19, n = 1.0 ± 0.2; Ba^{2+} (empty squares), $K_{1/2}$ = 4.8 ± 0.6, n = 0.9 ± 0.1.

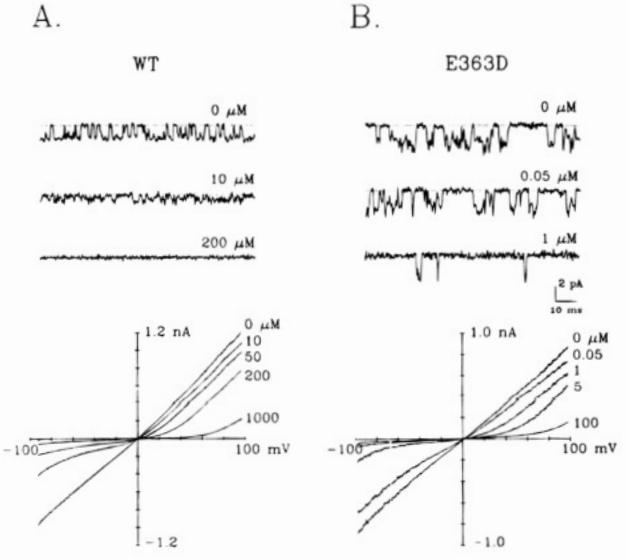

FIGURE 6: E363D mutation increases blocker affinity by decreasing its rate of dissociation. (A) Single channel (top) and multichannel (bottom) currents were recorded for wild type channels in the presence of different concentrations of extracellular Sr^{2+}. The single channel patch was held at −80 mV, and the multichannel patch was ramped between −100 and 100 mV. (B) Similar recordings are shown for the E363D mutant channel.

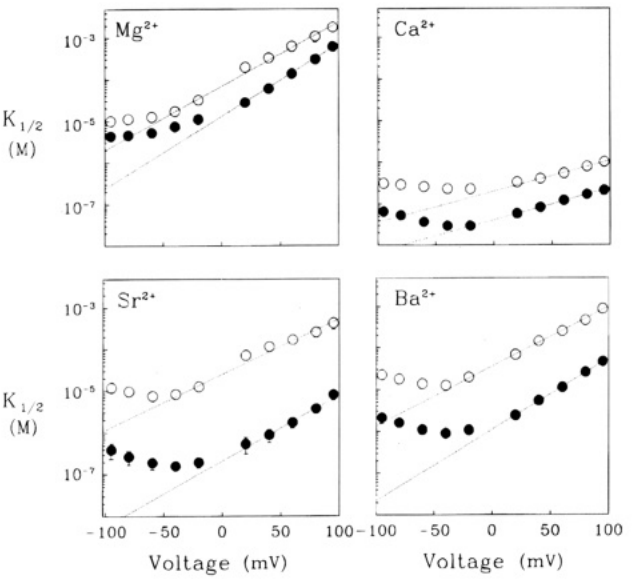

FIGURE 7: Effect of the E363D mutation on blocker affinity is proportional at all membrane voltages. $K_{1/2}$ for blockade of the wild type channel (empty circles) and the E363D mutant channel (filled circles) is plotted as a function of membrane voltage for the indicated ions. The lines correspond to the blocking equation $K_{1/2} = K_{1/2}(0\text{ mV})\exp(z\delta FV/RT)$. $K_{1/2}(0\text{ mV})$ in micromolar and δ (in parentheses) for the wild type and mutant channels are as follows: Mg^{2+}, 69 (0.46), 13 (0.52); Ca^{2+}, 0.200 (0.22), 0.041 (0.23); Sr^{2+}, 25 (0.40), 0.21 (0.47); Ba^{2+}, 36 (0.43), 1.1 (0.51).

for each blocking ion, meaning the selectivity has been altered.

DISCUSSION

The divalent cation binding site in the wild type CNG channel shows a definite preference for Ca^{2+} ions. By measuring blockade at positive membrane voltages, where extracellular divalent cations are near equilibrium with the site, we have estimated the affinity as a function of ionic radius. In addition to being the ion with the highest affinity, Ca^{2+} is unique in two other respects. The voltage dependence, which is nearly the same for Mg^{2+}, Sr^{2+}, and Ba^{2+}, is much lower for Ca^{2+}. Also, Ca^{2+} blocks with a high Hill coefficient, implying that more than one may enter the pore.

A graph of the half-blocking concentration, $K_{1/2}$, plotted as a function of ionic radius is shown in Figure 8A. The profile of selectivity for the wild type channel is unusual compared to those of other Ca^{2+} binding proteins; except for Ca^{2+}, there is no size selectivity. A typical EF-hand Ca^{2+} binding site shows a more gradual size selectivity (Falke et al., 1994). In the EF-hand of galactose binding protein, a minimum in binding energy occurs at Ca^{2+} because the smaller Mg^{2+} is more strongly hydrated and the larger Sr^{2+} does not fit optimally into the rigid binding cavity (Snyder et al., 1990; Falke et al., 1991). As one would expect, the even larger Ba^{2+} binds more weakly than Sr^{2+}. The binding site in the wild type CNG channel does not follow this trend in the large ion limit. Nonselective binding sites known as carboxylate clusters have been described (Needham et al., 1993). They coordinate the ion on only one hemisphere; water molecules solvate the other half (Stock et al., 1993). The binding site in the channel functionally appears to be intermediate between these two extremes; it is not selective among Mg^{2+}, Sr^{2+}, and Ba^{2+} but it does select for Ca^{2+}.

In order to explain this selectivity pattern, we invoke the possibility that Ca^{2+} binds in a different manner or in a

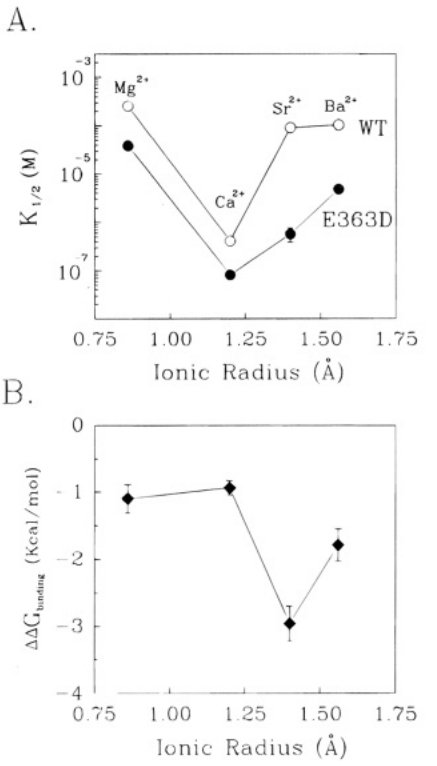

FIGURE 8: E363D mutation shifts divalent cation selectivity toward larger ions. (A) Half-blocking concentration ($K_{1/2}$) values of four divalent cations measured at 30 mV are shown for the wild type (empty circles) and the E363D mutant (filled circles) channels as a function of their ionic radius. (B) The difference in free energy of binding ($\Delta\Delta G = RT \ln K_{1/2}(\text{E363D})/K_{1/2}(\text{WT})$) to the wild type versus the mutant channel is shown for each ion.

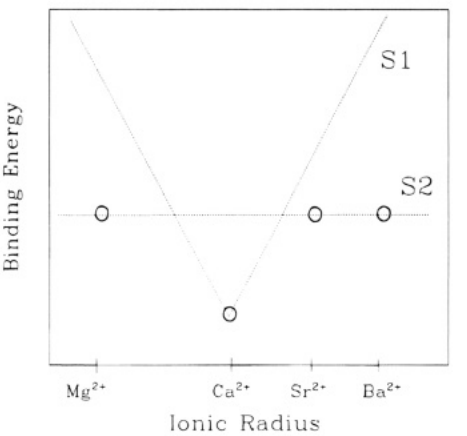

FIGURE 9: Energy as a function of ionic radius for two hypothetical divalent cation binding sites (dashed lines). S1 corresponds to a size-selective coordination cage as is found in EF-hand binding sites. S2 corresponds to a nonselective site (i.e. carboxylate cluster). Circles indicate the preferred binding site for each divalent cation if both sites are present in the pore of the wild type channel.

different position than the other ions. For the sake of argument, imagine that the pore has two binding sites, one that forms a cage (S1) and is selective (analogous to an EF-hand) and another that is like a carboxylate cluster and therefore is nonselective (S2). These could be two distinct sites, or they could represent different configurations of the same amino acids. When an ion enters the pore, it could bind to either site (or in either configuration). If the size selectivity and affinities of the two sites are given by Figure 9, when a Ca^{2+} enters, it would bind in S1 while the other ions would bind preferentially in S2. This hypothesis of two

kinds of sites in the pore is of course speculative, but it unifies several separate functional properties of blockade in the wild type channel. First, it offers an explanation for the unusual "strict" Ca^{2+} selectivity in the setting of nonselectivity among the other ions. Second, a different site for Ca^{2+} would explain why it blocks with a unique voltage dependence. Third, two (or more) sites would explain the high Hill coefficient for Ca^{2+} blockade. Multiple sites would potentially be available for the other ions, but due to the selectivity of S1, it would not be occupied by ions other than Ca^{2+}. Therefore, the other ions would have a Hill coefficient closer to unity.

The effects of the chemically conservative mutation E363D point to the importance of these residues in divalent cation selectivity in the pore. The affinity of Sr^{2+} and Ba^{2+} is increased more than those of Mg^{2+} and Ca^{2+} so that selectivity is shifted in the direction of larger ions (Figure 8B). The pattern of a gradual decrease in affinity as ion size is increased from Ca^{2+} to Ba^{2+} becomes more consistent with classical size selectivity. We are not able to extract a mechanistic explanation for these changes in ion binding, but we speculate that the shorter side chain on Asp could allow larger ions to fit more optimally. Nevertheless, the mutation highlights the importance of the Glu residues in determining the divalent cation selectivity of this channel.

ACKNOWLEDGMENT

We thank Z. Lu and M. Root for their critical review and comments on the manuscript.

REFERENCES

Chen, T. Y., Peng, Y. W., Dhallan, R. S., Ahamed, B., Reed, R. R., & Yau, K. W. (1993) *Nature (London) 362*, 764−767.

Colamartino, G., Menini, A., & Torre, V. (1991) *J. Physiol. 440*, 189−206.

Eismann, E., Muller, F., Heinemann, S. H., & Kaupp, U. B. (1994) *Proc. Natl. Acad. Sci. U.S.A. 91*, 1109−1113.

Falke, J. J., Snyder, E. E., Thatcher, K. C., & Voertler, C. S. (1991) *Biochemistry 30*, 8690−8697.

Falke, J. J., Drake, S. K., Hazard, A. L., & Falke, J. J. (1994) *Q. Rev. Biophys. 27*, 219−290.

Goulding, E. H., Ngai, J., Kramer, R. H., et al. (1992) *Neuron 8*, 45−58.

Goulding, E. H., Tibbs, G. R., Liu, D., & Siegelbaum, S. A. (1993) *Nature (London) 364*, 61−64.

Karpen, J. W., Brown, R. L., Stryer, L., & Baylor, D. A. (1993) *J. Gen. Physiol. 101*, 1−25.

Kaupp, U. B., & Koch, K.-W. (1991) *Annu. Rev. Physiol. 54*, 153−175.

Kaupp, U. B., Niidome, T., Tanabe, T., et al. (1989) *Nature (London) 342*, 762−766.

Koutalos, Y., & Yau, K.-W. (1993) *Curr. Opin. Neurobiol. 3*, 513−519.

Liman, E. R., Tytgat, J., & Hess, P. (1992) *Neuron 9*, 861−871.

MacKinnon, R. (1995) *Neuron 14*, 889−892.

Martell, A. E., & Smith, R. M. (1974) in *Critical Stability Constants*, Vol. 1, pp 204−271, Plenum Press, New York.

Menini, A., Rispoli, G., & Torre, V. (1988) *J. Physiol. 402*, 279−300.

Needham, J. V., Chen, T. Y., & Falke, J. J. (1993) *Biochemistry 32*, 3363−3367.

Root, M. J., & MacKinnon, R. (1993) *Neuron 11*, 459−466.

Snyder, E. E., Buoscio, B. W., & Falke, J. J. (1990) *Biochemistry 29*, 3937−3943.

Stern, J. H., Knutsson, H., & MacLeish, P. R. (1987) *Science 236*, 1674−1678.

Stock, A. M., Martinez-Hackert, E., Rasmussen, B. F., et al. (1993) *Biochemistry 32*, 13375−13380.

Wolf, H. U. (1973) *Experientia 29/2*, 242−249.

Woodhull, A. M. (1973) *J. Gen. Physiol. 61*, 687−708.

Yau, K.-W., & Baylor, D. A. (1989) *Annu. Rev. Neurosci. 12*, 289−327.

Yau, K.-W., & Chen, T.-Y. (1995) Cyclic nucleotide-gated channel, in *Handbook of Receptors and Channels - Ligand and voltage gated ion channel* (North, R. A., Ed.) pp 307−335, CRC Press, Boca Raton, FL.

Zimmerman, A. L., & Baylor, D. A. (1992) *J. Physiol. 449*, 759−783.

BI951324G